A depth-averaged grain-fluid model with dilatancy and an upper-solid layer

François Bouchut[1*], *Enrique D.* Fernández-Nieto[2,**], *Anne* Mangeney[3,***], and *Gladys* Narbona-Reina[2,****]

[1]Laboratoire d'Analyse et de Mathématiques Appliquées, Université Gustave Eiffel, CNRS-UMR 8050, F-77454, Marne-la-Vallée, France.
[2]Departamento Matemática Aplicada I, Universidad de Sevilla. E.T.S. Arquitectura. Avda, Reina Mercedes, s/n. 41012 Sevilla, Spain.
[3]Institut de Physique du Globe de Paris, Université Paris Cité, CNRS-UMR 7154, 1 rue Jussieu, 75005 Paris, France.

Abstract. To effectively assess the growing hazard related to debris flows, it is crucial to simulate these natural grain-fluid flows at a reasonable computational cost. To complement existing depth-averaged grain-fluid flow models with an upper-fluid layer, we propose here a model with an upper-solid layer, as a first step towards the development of unified models describing all possible configurations. This model accounts for granular mass dilatancy and pore fluid pressure feedback and solves for solid and fluid velocity in the mixture and for the upper-solid velocity. Simulation in uniform configurations reveals the rich behaviour of the flow and shows that the upper-solid and upper-fluid models may predict very different behaviour. Our work highlights the need of developing two-layer models accounting for dilatancy and unifying upper-solid and upper-fluid configurations in the same framework.

1 Introduction

The risks associated with landslides and debris flows have considerably increased with climate change and population growth. Landslide and debris flow models are used for hazard assessment to simulate possible scenarios and predict the impact of these grain-fluid flows in terms of runout distance, maximal flow heights, impact pressure or velocities. To prevent high computational cost, most landslide models are based on the depth-averaged shallow approximation that assumes that the landslide flow thickness is small compared to its downslope extension [1–3].

Landslide and debris flow simulations with these models are however highly uncertain because of the absence of realistic description of the grain-fluid interactions, in particular dilatancy, which play a key role on the dynamics and deposit properties of these events. The dilation/contraction of the solid phase that decrease/increase the pore fluid pressure with strong feedback on the friction experienced by the granular phase has been shown to dramatically change the dynamics of the grain-fluid mixture, possibly leading to its complete liquefaction [3–6].

[4] revisited by [7] proposed a two-phase model with an upper-fluid layer capable of collecting or providing water during contraction or dilation of the mixture. However, this model does not describe the situation where the upper layer is only made of grains. Such a configuration has been studied in [8], where a depth-averaged model is proposed, dealing with transitions from pure fluid/solid configurations to under-saturated or over-saturated mixtures. However, this model does not account for dilatancy or mass exchange. [9] developed a model, accounting for dilatancy, that deals with all the possible configurations (fluid, solid and a mixture with either an upper-fluid or upper-solid layer) by switching between the resolution of the corresponding systems of equations. However, the unknowns change from one system of equations to the other. We thus lack a more unified framework to describe all configurations in debris flows.

Our objectives here are to (i) present the upper-solid version (Figure 1) of the upper-fluid model derived in [4], as a first step towards the development of a unified model for debris flows, and (ii) show simple simulations in uniform setting to get insight into the model behaviour. In section 2 we propose a layer-averaged model with an upper-solid layer including the $\mu(\mathcal{J})$ rheology and dilatancy laws derived from critical state mechanics. Then, in section 3, we present first numerical simulations of uniform flows with this model.

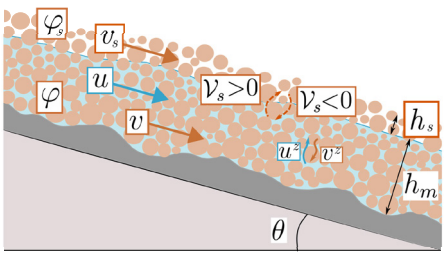

Figure 1. Flow configuration and notation of the mixture model with an upper-solid layer.

*e-mail: francois.bouchut@univ-eiffel.fr
**e-mail: edofer@us.es
***e-mail: mangeney@ipgp.fr
****e-mail: gnarbona@us.es

2 Depth-averaged grain-fluid model with an upper-solid layer

We present the depth-averaged model describing an upper-solid layer on top of a mixture made of solid and fluid phases (Figure 1). Our model complements the depth-averaged upper-fluid model proposed in [4] and revisited in [7]. We prescribe rheological and dilatancy laws [4, 10]. To do that we follow [7] by using the $\mu(\mathcal{J})$ rheology and the dilatancy laws proposed by [11] and by [12, 13], respectively. These laws are given below.

The notations are the following. In the mixture domain, flow thickness is denoted by h_m, the fluid variables are written with a subscript $()_{f_m}$, and solid variables are written with a subscript $()_{s_m}$. The upper-solid domain has thickness h_s, and the subscript $()_s$ is used for the variables. The constant densities of the fluid and solid phases are denoted by ρ_f and ρ_s, respectively.

We use the shallow approximation and depth-average the 3D Jackson's equations within both the grain-fluid and the upper solid layers [14]. The interface that separates these two layers corresponds to the fluid surface. The resulting shallow depth-averaged model accounts for 8 unknowns, five scalars, namely the mixture and upper solid thicknesses h_m, h_s, the mixture and upper solid depth-averaged solid volume fraction φ, φ_s, the solid volume flux that is transferred between the mixture and the upper layer $\mathcal{V}_s$, and the 3 depth-averaged vectorial velocities for the solid and fluid phases in the mixture $\mathbf{v}, \mathbf{u}$, and for the solid phase in the upper layer $\mathbf{v}_s$. The proposed system states as follows, for the mass conservation

$$\partial_t(\rho_f(1-\varphi)h_m) + \nabla\cdot(\rho_f(1-\varphi)h_m\mathbf{u}) = 0 \tag{1a}$$
$$\partial_t(\rho_s\varphi h_m) + \nabla\cdot(\rho_s\varphi h_m\mathbf{v}) = -\rho_s\mathcal{V}_s \tag{1b}$$
$$\partial_t(\rho_s\varphi_s h_s) + \nabla\cdot(\rho_s\varphi_s h_s\mathbf{v}_s) = \rho_s\mathcal{V}_s, \tag{1c}$$

for the evolution of the solid volume fractions

$$\partial_t\varphi + \mathbf{v}\cdot\nabla\varphi = -\varphi\Phi \tag{2a}$$
$$\partial_t\varphi_s + \mathbf{v}_s\cdot\nabla\varphi_s = -\varphi_s\Phi_s, \tag{2b}$$

and for the momentum conservation

$$\partial_t(\rho_f(1-\varphi)h_m\mathbf{u}) + \nabla\cdot(\rho_f(1-\varphi)h_m\mathbf{u}\otimes\mathbf{u}) = S_u^{\mathrm{fm}} \tag{3a}$$
$$\partial_t(\rho_s\varphi h_m\mathbf{v}) + \nabla\cdot(\rho_s\varphi h_m\mathbf{v}\otimes\mathbf{v}) = S_v^{\mathrm{sm}} \tag{3b}$$
$$\partial_t(\rho_s\varphi_s h_s\mathbf{v}_s) + \nabla\cdot(\rho_s\varphi_s h_s\mathbf{v}_s\otimes\mathbf{v}_s) = S_{v_s}^{s}. \tag{3c}$$

The source terms in the momentum equations are given respectively by

$$\begin{aligned} S_u^{\mathrm{fm}} = \;& -\rho_f g\cos\theta(1-\varphi)h_m\nabla(b+h_m) - (1-\varphi)h_m\overline{\nabla p^e_{f_m}} \\ & -\beta h_m(\mathbf{u}-\mathbf{v}) - k_s(\mathbf{u}-\mathbf{v}_s) - \frac{5}{2}\frac{\eta_e(1-\varphi)}{h_m}\mathbf{u} \\ & -(1-\varphi)h_m\rho_f g\sin\theta\mathbf{e}_x, \end{aligned}$$

$$\begin{aligned} S_v^{\mathrm{sm}} = \;& -(\rho_s-\rho_f)g\cos\theta\frac{h_m^2}{2}\nabla\varphi \\ & -\rho_s g\cos\theta h_m(\varphi\nabla(b+h_m) + \nabla(\varphi_s h_s)) \\ & +(1-\varphi)h_m\overline{\nabla p^e_{f_m}} - \Big(\lambda_s\mathbf{v}_s + (1-\lambda_s)\mathbf{v}\Big)\rho_s\mathcal{V}_s \\ & +\beta h_m(\mathbf{u}-\mathbf{v}) + \mu_s\,\mathrm{sgn}(\mathbf{v}_s-\mathbf{v})(\rho_s g\cos\theta\varphi_s h_s) \\ & -\mu\,\mathrm{sgn}(\mathbf{v})\Big(g\cos\theta((\rho_s-\rho_f)\varphi h_m + \rho_s\varphi_s h_s) \\ & -(p^e_{f_m})_{|b}\Big) - \varphi h_m\rho_s g\sin\theta\mathbf{e}_x, \end{aligned}$$

$$\begin{aligned} S_{v_s}^{s} = \;& -\rho_s g\cos\theta h_s\Big(\varphi_s\nabla(b+h_m+h_s) + \frac{h_s}{2}\nabla\varphi_s\Big) \\ & +\Big(\lambda_s\mathbf{v}_s + (1-\lambda_s)\mathbf{v}\Big)\rho_s\mathcal{V}_s + k_s(\mathbf{u}-\mathbf{v}_s) \\ & -\mu_s\,\mathrm{sgn}(\mathbf{v}_s-\mathbf{v})\Big(\rho_s g\cos\theta\varphi_s h_s\Big) \\ & -\rho_s g\sin\theta\varphi_s h_s\mathbf{e}_x, \end{aligned}$$

with a drag coefficient k_s between the grains in the upper layer and the fluid in the mixture, and $\eta_e = \eta_f(1+\frac{5}{2}\varphi)$ the effective viscosity with η_f the dynamic viscosity of the fluid. The drag coefficient β is defined as in [15]

$$\beta = (1-\varphi)^2\frac{\eta_f}{k} \quad \text{with} \quad k = \frac{(1-\varphi)^3 d^2}{150\varphi^2}, \tag{4}$$

where d is the grain diameter and k the hydraulic permeability of the granular aggregate. The quantities related to the excess pore pressure appearing in the model are defined by

$$\overline{\nabla p^e_{f_m}} = \frac{1}{h_m}\Big(\nabla(h_m\overline{p^e_{f_m}}) + (p^e_{f_m})_{|b}\nabla b\Big), \tag{5}$$

with the basal excess pore pressure

$$(p^e_{f_m})_{|b} = -\frac{\beta}{(1-\varphi)^2}\frac{h_m^2}{2}\Phi, \quad \overline{p^e_{f_m}} = -\frac{\beta}{(1-\varphi)^2}\frac{h_m^2}{3}\Phi, \tag{6}$$

with Φ defined by the dilatancy laws

$$\begin{aligned} &\Phi = \dot\gamma\tan\psi,\ \tan\psi = K(\varphi-\varphi^{\mathrm{eq}}) && \text{in the mixture,} \\ &\Phi_s = \dot\gamma_s\tan\psi_s,\ \tan\psi_s = K(\varphi_s-\varphi_s^{\mathrm{eq}}) && \text{in the upper-layer,} \end{aligned} \tag{7}$$

where ψ, ψ_s are the dilatation angles and K is an empirical constant.

The rheological law for the solid in the mixture that defines the critical-state friction coefficient μ^{eq} and the critical-state solid volume fraction φ^{eq} as a function of the inertial number I and the viscous numbers J reads

$$\begin{aligned} &\mu = (\mu^{\mathrm{eq}} + K(\varphi-\varphi^{\mathrm{eq}}))_+, \\ &\text{with} \quad \mu^{\mathrm{eq}} = \mu_c + \frac{\Delta\mu}{1+I_0/\mathcal{J}_\mu^{1/2}} \quad \text{and} \quad \mathcal{J}_\mu = \alpha_\mu I^2 + J, \\ &\varphi^{\mathrm{eq}} = \frac{\varphi_c}{1+b_\varphi\mathcal{J}_\varphi^{1/2}}, \quad \text{with} \quad \mathcal{J}_\varphi = \alpha_\varphi I^2 + J, \\ &\text{where} \quad I = \frac{d\,\dot\gamma}{\sqrt{p_{s_{m|b}}/\rho_s}}, \quad J = \frac{\eta_f\dot\gamma}{p_{s_{m|b}}}, \quad \text{with} \quad \dot\gamma = \frac{5}{2}\frac{|\mathbf{v}|}{h_m} \\ &\text{and } p_{s_{m|b}} = g\cos\theta(\rho_s\varphi_s h_s + (\rho_s-\rho_f)\varphi h_m) - (p^e_{f_m})_{|b}. \end{aligned}$$

Here $\mu_c = \tan\delta$ is the static value of the critical state friction coefficient, with δ the granular friction angle, and φ_c is the static value of the critical state solid volume fraction. Finally $\Delta\mu$, I_0, b_φ, α_φ and α_μ are constant parameters [11]. For the solid upper-layer the rheology reads

$$\begin{aligned} &\mu_s = \Big(\mu_s^{\mathrm{eq}} + K(\varphi_s-\varphi_s^{\mathrm{eq}})\Big)_+, \\ &\text{with} \quad \mu_s^{\mathrm{eq}}(I_s) = \mu_c + \frac{\Delta\mu}{1+I_0/I_s}, \quad \varphi_s^{\mathrm{eq}}(I_s) = \frac{\varphi_c}{1+b_\varphi I_s}, \\ &\text{where} \quad I_s = \frac{d\,\dot\gamma_s}{\sqrt{p_{s|i}/\rho_s}}, \quad \dot\gamma_s = \frac{5}{2}\frac{|\mathbf{v}_s|}{h_s}, \\ &\text{and} \quad p_{s|i} = \varphi_s\rho_s g\cos\theta h_s. \end{aligned} \tag{8}$$

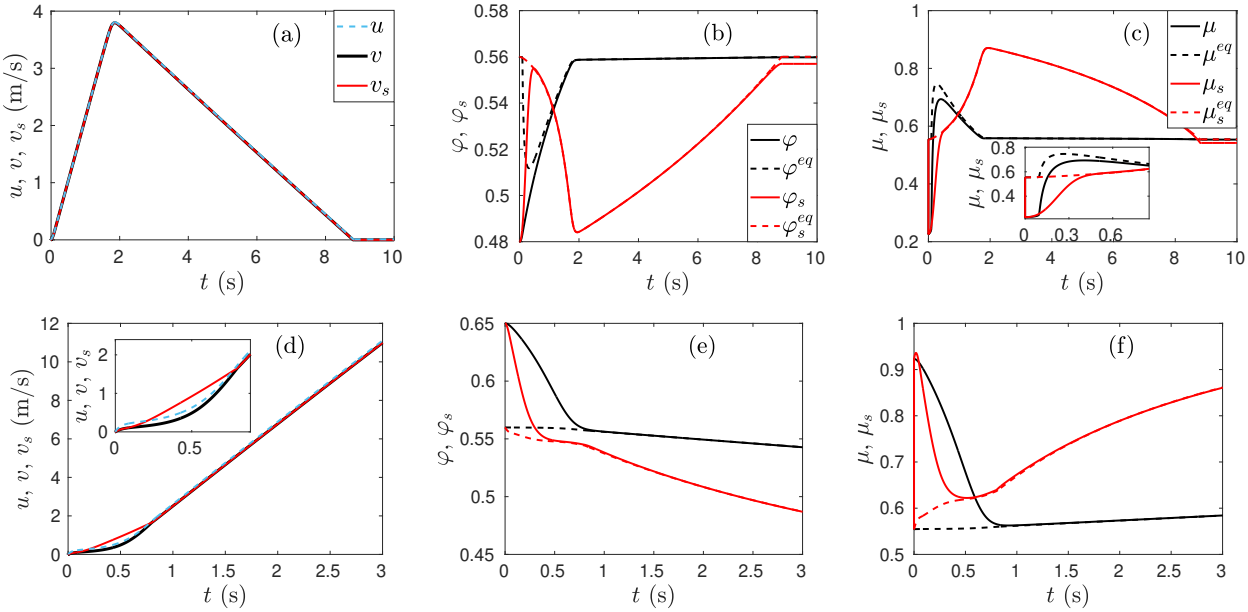

Figure 2. Simulations in the loose (first line) and dense (second line) cases. Left: solid and fluid velocities u and v in the mixture and upper-solid velocity v_s; middle: solid volume fractions in the mixture φ and in the upper-solid layer φ_s and the corresponding values at the critical state φ^{eq} and φ_s^{eq}; right: friction coefficients μ, μ_s and the their values at the critical state μ^{eq} and μ_s^{eq}. The mixture variables are in black and the upper-solid variables in red.

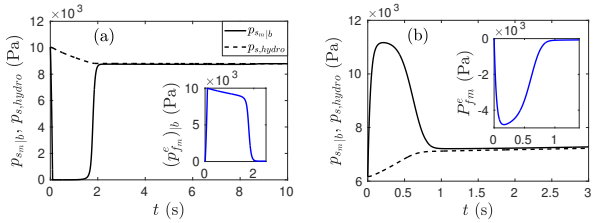

Figure 3. Solid pressure $p_{s_m|b}$ and hydrostatic pressure $p_{s_m,hydro}$ at the bed (insert excess pore fluid pressure p^e_{fm}) (a) in the loose and (b) dense cases.

The transference term through the interface between the two layers, deduced from equations (1)-(2), reads

$$\frac{1-\varphi}{\varphi}\mathcal{V}_s = h_m\Phi + \nabla\cdot(h_m(1-\varphi)(\mathbf{u}-\mathbf{v})). \qquad (9)$$

The distribution coefficient is

$$\lambda_s = \frac{1}{2}-\frac{1}{2}\,\mathrm{sgn}(\mathcal{V}_s)\delta_s;\ \delta_s = \begin{cases} 0 & \text{centered approximation,} \\ 1 & \text{upwind approximation.} \end{cases} \qquad (10)$$

3 Numerical Results

We perform here simple tests in uniform setting to get insight into the rich dynamics of these grain-fluid flows. Following [7], the material properties are set to $\rho_f = 1000\,\mathrm{kg/m^3}$, $\rho_s = 2700\,\mathrm{kg/m^3}$, $\eta_f = 10^{-3}$ Pa s, and the rheological parameters to $\alpha_\varphi = 0.1$, $\alpha_\mu = 0.0088$, $b_\varphi = 0.99$, $I_0 = 0.279$, $\mu_c = \tan 29°$, $\varphi_c = 0.56$, $a_\mu = 5.645$, $\Delta\mu = \mu_c a_\mu I_0$, $K = 4.09$ and $k_s = 0$.

We release granular materials initially at rest ($v^0 = u^0 = v_s^0 = 0$ m/s) in two cases: an initially loose and an initially dense uniform granular layer. The initial thickness of the mixture h_m^0, the initial thickness of the upper-solid layer defined as a fraction C_h of the mixture thickness $h_s^0 = C_h h_m^0$, and the initial solid volume fractions are

$$\begin{cases} h_m^0 = 0.7169\,\mathrm{m}, & \varphi^0 = 0.48, & C_h = 0.5, & \text{loose case,} \\ h_m^0 = 0.65\,\mathrm{m}, & \varphi^0 = 0.59, & C_h = 0.15, & \text{dense case.} \end{cases}$$

The slope angle of the bottom and grain diameter are set to $\theta = 13°$ and $d = 10^{-3}$ m for the loose case and to $\theta = 45°$ and $d = 3.10^{-3}$ m for the dense case. We consider the same mass for the mixture in the loose and dense cases so that $(\rho^0 h_m^0)_{\text{loose}} = (\rho^0 h_m^0)_{\text{dense}}$. We observe the typical behaviours of intially loose and initially dense layers [7]. Note that the parameters for the loose case are the same than in the simulations shown in Figure 11 of [7], obtained with the upper-fluid model.

In the loose case (see Figures 2a-c and 3a), the material initially compresses in both the mixture and the upper-solid layers. In the mixture layer, this compression induces an increase of the excess pore fluid pressure that drastically reduces the solid pressure down to almost zero (Figure 3a). On top of that the friction coefficient decreases due to the large negative values of the tangent of the dilation angle ψ. These combined effects make the friction force almost disappear and the solid velocity in the mixture thus rapidly increases. As these processes are obviously not present in the dry upper-solid layer and because the slope is much smaller than the friction angle, the upper layer would have stay at rest if it would not have been entrained by the mixture layer. Indeed the friction between these two layers make the upper layer move even at such small slope angle. The behaviour of φ and φ_s are observed to be quite different. The solid volume fractions in the two layers first increases due to compression and φ_s very rapidly reaches the critical volume fraction φ_s^{eq} while it takes about 2 s for φ to reach φ^{eq}. At that time, when compression disappears, the pressure goes back to hydrostatic and the friction force makes the flow slow down (Figure 2a). Interestingly, up to 2 s the behaviour obtained with

the upper-solid model is close to the one simulated with the upper-fluid model [7] even if the velocities are smaller. Afterwards, the mass decelerates and stops at $t \simeq 8.5$ s with the upper-solid model while it accelerates with the upper-fluid model due to the entrainment of the upper-fluid layer. Otherwise, the evolution of the pressures and of the friction coefficient in the mixture is qualitatively similar in both models. Note that due to the small grain diameter $d = 10^{-3}$, the friction between the solid and fluid phases in the mixture is high (equation (4)) and the mixture solid and fluid velocities are almost the same since the very beginning.

In the dense case, the material initially dilates in both the mixture and the upper-solid layers (Figure 2e). In the mixture layer, this dilation induces a negative pore fluid pressure and thus an increase of the friction force due to increasing solid pressure (Figure 3b). As a result, for about 0.5 s which corresponds to the duration of large dilation, the velocity of the mixture is still very small despite the high slope angle ($\theta = 45°$), while the velocity of the solid upper-layer starts to grow. As the dilation decreases, the solid velocity in the mixture starts to increase too. It reaches the velocity of the upper-solid layer at about 0.8 s, once the solid volume fraction in the mixture reaches the critical volume fraction and thus once the dilation goes to zero. After this time we see that φ_s decreases more than φ due to the different behaviour of φ_s^{eq} and φ^{eq}. It is worth pointing out that, despite the small grain diameter which induces a high friction between the grains and the fluid in the mixture, the fluid velocity $\mathbf{u}$ at the very beginning is slightly higher than the solid velocity $\mathbf{v}$.

4 Conclusion

The upper-solid model presented here complements the upper-fluid model proposed by [4, 7]. We show that the flow behaviour may be significantly different from the upper-fluid model with the same parameters (layer thicknesses, slope, material and rheological parameters) as observed in the loose case presented here, when compared with the results of [7]. This suggests that mixture models with a virtual layer as those of [3, 16] may be too rough to simulate grain-fluid flows, at least when the upper-layer thickness is large. This work support the need of developing unified models describing all possible configuration from pure solid, pure fluid to mixtures with an upper fluid-layer or an upper solid-layer.

Funding. This work was supported by the European projects ERC-CG-2013-PE10-617472 SLIDEQUAKES and DT-GEO, and part of the MSCA Doctoral Network EnvSeis consortium (101073148). It is also funded by the National Spanish (PID2022-137637NB-C22), MCIN/AEI/10.13039/501100011033, by "ERDF A way of making Europe" and by Junta de Andalucía, Spain research project ProyExcel 00525.

References

[1] A. Lucas, A. Mangeney, J.P. Ampuero, Frictional velocity-weakening in landslides on earth and on other planetary bodies, Nature Communications **5** (2014).

[2] S.B. Savage, K. Hutter, The motion of a finite mass of granular material down a rough incline, Journal of Fluid Mechanics **199**, 177 (1989).

[3] R.M. Iverson, D.L. George, A depth-averaged debris-flow model that includes the effects of evolving dilatancy. I. Physical basis, Proceedings of the Royal Society A: Mathematical, Physical and Engineering Sciences **470**, 20130819 (2014).

[4] F. Bouchut, E.D. Fernández-Nieto, A. Mangeney, G. Narbona-Reina, A two-phase two-layer model for fluidized granular flows with dilatancy effects, Journal of Fluid Mechanics **801**, 166 (2016).

[5] L. Rondon, O. Pouliquen, P. Aussillous, Granular collapse in a fluid: Role of the initial volume fraction, Physics of Fluids **23**, 073301 (2011).

[6] F. Bouchut, E. Fernández-Nieto, E. Koné, A. Mangeney, G. Narbona-Reina, Dilatancy in dry granular flows with a compressible $\mu(i)$ rheology, Journal of Computational Physics **429**, 110013 (2021).

[7] F. Bouchut, E. Drach, E.D. Fernández-Nieto, A. Mangeney, G. Narbona-Reina, A series of two-phase models for grain-fluid flows with dilatancy, Journal of Fluid Mechanics **(in press)** (2025).

[8] X. Meng, A. Taylor-Noonan, C. Johnson, W. Take, E. Bowman, J. Gray, Granular-fluid avalanches: the role of vertical structure and velocity shear, Journal of Fluid Mechanics **980**, A11 (2024).

[9] W. Sun, Y. Wang, Modeling phase separation in grain-fluid mixture flows by a depth-averaged approach with dilatancy effects, Journal of Geophysical Research: Earth Surface **129**, e2023JF007416 (2024).

[10] F. Bouchut, E.D. Fernández-Nieto, A. Mangeney, G. Narbona-Reina, A two-phase shallow debris flow model with energy balance, ESAIM: M2AN **49**, 101 (2015).

[11] F. Tapia, M. Ichihara, O. Pouliquen, E. Guazzelli, Viscous to inertial transition in dense granular suspension, Phys. Rev. Lett. **129**, 078001 (2022).

[12] S. Roux, F. Radjai, Texture-Dependent Rigid-Plastic Behavior (Springer Netherlands, Dordrecht, 1998), pp. 229–236, ISBN 978-94-017-2653-5

[13] M. Pailha, M. Nicolas, O. Pouliquen, Initiation of underwater granular avalanches: Influence of the initial volume fraction, Physics of Fluids **20**, 111701 (2008).

[14] R. Jackson, The Dynamics of Fluidized Particles (Cambridges Monographs on Mechanics. Cambridge University Press, 2000)

[15] M. Pailha, O. Pouliquen, A two-phase flow description of the initiation of underwater granular avalanches, Journal of Fluid Mechanics **633**, 115 (2009).

[16] X. Meng, Y. Wang, Modeling dynamic flows of grain–fluid mixtures by coupling the mixture theory with a dilatancy law, Acta Mech **229**, 2521 (2018).